

## Phase behavior of ultrasoft spheres show stable bcc lattices

A. Scotti <sup>1</sup>, J. E. Houston <sup>2</sup>, M. Brugnoli <sup>1</sup>, M. M. Schmidt <sup>1</sup>, M. F. Schulte <sup>1</sup>,  
S. Bochenek <sup>1</sup>, R. Schweins <sup>3</sup>, A. Feoktystov <sup>4</sup>, A. Radulescu <sup>4</sup>, and W. Richtering <sup>1,5</sup>

<sup>1</sup>*Institute of Physical Chemistry, RWTH Aachen University, 52056 Aachen, Germany*

<sup>2</sup>*European Spallation Source ERIC, Box 176, SE-221 00 Lund, Sweden*

<sup>3</sup>*Institut Laue-Langevin ILL DS/LSS, 71 Avenue des Martyrs, F-38000 Grenoble, France*

<sup>4</sup>*Forschungszentrum Jülich GmbH, Jülich Centre for Neutron Science JCNS at Heinz Maier-Leibnitz Zentrum MLZ, 85748 Garching, Germany*

<sup>5</sup>*JARA-SOFT, 52056 Aachen, Germany*



(Received 15 July 2020; accepted 1 October 2020; published 2 November 2020)

The phase behavior of supersoft spheres is explored using solutions of ultralow cross-linked poly(*N*-isopropylacrylamide)-based microgels as a model system. For these microgels, the effects of the electric charges on their surfaces can be neglected and therefore only the role of softness on the phase behavior is investigated. The samples show a liquid-to-crystal transition at higher volume fraction with respect to both hard spheres and stiffer microgels. Furthermore, stable body centered cubic (bcc) crystals are observed in addition to the expected face centered cubic (fcc) crystals. Small-angle x-ray and neutron scattering with contrast variation allow the characterization of both the microgel-to-microgel distance and the architecture of single microgels in crowded solutions. The measurements reveal that the stable bcc crystals depend on the interplay between the collapse and the interpenetration of the external shell of the ultralow cross-linked microgels.

DOI: [10.1103/PhysRevE.102.052602](https://doi.org/10.1103/PhysRevE.102.052602)

Colloidal dispersions are suitable model systems to reproduce the behavior of atomic systems and complex fluids. For instance, the possibility to have entropy-driven phase transitions was largely debated in the condensed matter community and was only predicted theoretically [1–3]. The entropy-driven formation of crystals was first proven by Pusey and van Megen in the late 1980s using a solution of polymethylmethacrylate (PMMA) hard spheres [4]. From this moment, colloidal dispersions have been largely used to explore phase transitions both in two and three dimensions [5–8]. The aforementioned studies used suspensions of hard incompressible colloids, which were sterically stabilized.

At the same time as the experiments of Pusey and van Megen, Pelton and Chibante synthesized monodisperse spherical cross-linked polymeric networks based on the monomer *N*-isopropylacrylamide (NIPAM) [9]. The resulting poly-*N*-isopropylacrylamide (pNIPAM)-based microgels have been largely used to explore phase transition and flow properties of soft spheres due to their colloidal size and intrinsic softness [10–18]. Indeed, softness (that is, the capability to deswell, deform, or interpenetrate) has a strong impact on the phase transitions and rheological properties of solutions of spheres. For instance, the boundary of the transition between liquid and crystalline phases are shifted to higher concentrations [19] as predicted by computer simulations [20]. Furthermore, size polydispersity suppresses the crystallization of hard spheres when it is as high as 12%. In contrast, solutions of soft microgels can crystallize even when the nominal size polydispersity is close to 20% [13]. This is due to the capability of microgels to adjust their size in response to variations in the osmotic

pressure of the solution [18]. In particular, larger microgels deswell first and fit into lattices composed of the smallest microgels without giving rise to defects [21,22].

It is worth noting that even if pNIPAM-based microgels are usually referred to as neutral, a significant amount of charges are incorporated at the microgel's periphery due to initiator fragments [23]. These charges, and the corresponding ions, play a fundamental role in determining the swelling behavior of microgels in concentrated solutions as shown both by experiments [13,18] and computer simulations [24,25].

Therefore, to study the phase behavior of truly neutral soft spheres, the number of charges on the microgel's surface has to be minimized. This can be achieved using the so-called ultralow cross-linked (ULC) microgels that are synthesized without the addition of cross-linker agents during the precipitation polymerization. The networks are formed via atom abstraction reactions during the polymerization of NIPAM initiated with a peroxydisulfate initiator [26]. During the synthesis of ULC microgels, many polymeric chains, and the associated charged fragments of the initiators, precipitate in the polymer globules but are not chemically attached to the network. These chains are washed out of the microgels during purification, which is confirmed by the very low yield of the precipitation polymerization of ULC microgels ( $\approx 10\%$ ) compared to the yield of regularly cross-linked microgels ( $\approx 90\%$ ). This means that the ULC microgels incorporate a lower amount of polymeric chains and associated charges, with respect to microgels synthesized with the use of a cross linker [27,28]. The lower surface charge of ULC microgels with respect to microgels synthesized with the addition of

cross linker is confirmed by measurements of their electrophoretic mobility shown in the Supplemental Material [29]. For these reasons, we can consider ultralow cross-linked microgels as almost neutral soft spheres. Details on the synthesis and the characterization of the swelling behavior of the ultralow cross-linked microgels used in this study with dynamic light scattering can be found in the Supplemental Material [29].

Because of their poorly cross-linked network, ULC microgels show a more pronounced deswelling behavior when embedded in a matrix of regularly crosslinked, stiffer microgels [28]. Furthermore, their bulk rheological properties present features in common with both hard spheres and flexible macromolecules, depending on the concentration of the solution [30]. This particle-to-polymer transition is also prominent when these ULC microgels are confined to an interface: The dominance of their polymeric or particle-like nature depends on both their concentrations [27] and the adsorption procedures [31].

In this study, we use solutions of ULC microgels to explore the phase behavior of soft spheres. The liquid-to-solid phase transition is shifted to higher generalized volume fraction with respect to both hard spheres and conventionally cross-linked microgels. Furthermore, the phase behavior shows a stable body centered cubic (bcc) lattice, which is not observed for other colloids. The coexistence of bcc lattice with face centered cubic (fcc) lattice, expected for hard spheres and other microgels, is rationalized by means of small-angle scattering experiments. We probe both the microgel-to-microgel arrangement in solution [x rays, small-angle x-ray scattering (SAXS)] and the structure of the single microgels as a function of concentration [neutrons, small-angle neutron scattering (SANS) with contrast variation]. The comparison between the results of these techniques shows that bcc crystals appear in the concentrations area where the collapse of the microgels competes with their capability to interpenetrate their neighbors.

### I. PHASE BEHAVIOR

At constant temperature and pressure, the quantity that determines the phase behavior of solutions of microgels is the volume occupied by the microgels in the solution; this is the volume fraction. In contrast to hard spheres that have a well-defined border and, therefore, volume, microgels have a fuzzy periphery that makes it hard to define their volume. It is well accepted that a generalized volume fraction can be used to describe the packing density of soft microgels [32–35]:

$$\zeta = \frac{NV_{sw}}{V_{tot}}, \quad (1)$$

where  $V_{tot}$  is the volume of the solution and  $N$  and  $V_{sw}$  are the number and the volume of the microgels in diluted solution, respectively.  $\zeta$  is connected to the weight concentration via a constant that can be obtained by measuring the viscosity of highly diluted solutions of microgels [19,36]. This method is also valid to determine the generalized volume fraction of ULC microgels [30].

A series of samples have been realized by successive dilution, starting from a microgel solution with  $\zeta = 1.50 \pm 0.02$ .

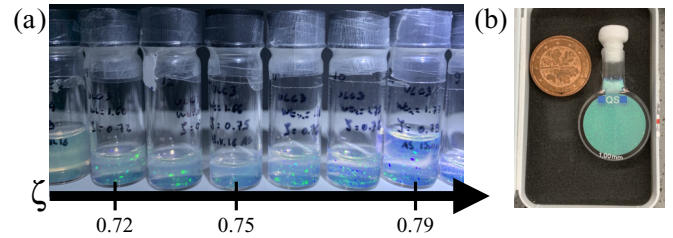


FIG. 1. (a) Solutions of ultralow cross-linked microgels with increasing generalized volume fraction,  $\zeta$ , from left to right. (b) Solution composed by a mixture of deuterated and hydrogenated ( $\zeta_H = 0.080 \pm 0.003$ ) ULC microgels at  $\zeta = 0.750 \pm 0.009$ . The iridescence due to the Bragg peaks is visible in crystalline samples. All samples were stored at  $20.0 \pm 0.5$  °C.

The starting solution was prepared adding bidistilled water to the microgel powder obtained from the lyophilization of the purified solution resulting from the synthesis (Supplemental Material [29]). The weight concentrations have been converted into generalized volume fractions using the conversion constant obtained from viscosity measurements,  $K = 44.9 \pm 0.01$ . The series of samples covers a range of  $\zeta$  between  $0.354 \pm 0.006$  and  $1.50 \pm 0.02$ .

The crystals formed in the solutions of ULC microgels are clearly visible by eye as green spots in Fig. 1(a). Crystals are not visible up to a concentration of  $\zeta_f = 0.717 \pm 0.09$  where they appear at the bottom of the vials and coexistence between crystals and liquid is observed.  $\zeta_f$  is known as freezing point. With increasing  $\zeta$ , the volume fraction of the solutions occupied by crystals increases linearly [12] until  $\zeta_m = 0.744 \pm 0.009$ . For this volume fraction, crystals are present in the entire volume of the solution.  $\zeta_m$  is called the melting point.

The values of  $\zeta_f$  and  $\zeta_m$  are significantly larger than the values usually observed for the freezing and melting points of solutions of microgels synthesized with the addition of cross-linker agents (referred to as regular microgels in the following): 0.56 and 0.61, respectively [13,19,35,37,38]. Computer simulations have shown that the shift of the boundaries of these phase transitions is related to a softer interaction potential acting between the microgels in solution [1,20].

The fact that  $\zeta_f$  and  $\zeta_m$  are at values larger than those for regular microgels indicates that the interaction between ULC microgels is softer. This fact is further confirmed by the increase of the elastic modulus of the solutions of ULC microgels with  $\zeta$ . The black squares in Fig. 2 are the values of  $G_p$ , the plateau of the elastic modulus, measured with oscillatory frequency sweep. Recently, it has been shown that a correct description of the microgel-to-microgel interaction can be achieved using a phenomenological multi-Hertzian model [39] that depends on the concentration regime and, therefore, on the different length scales that characterize the microgels [33,40]. However, a simple but instructive method to compare the softness of the microgel-to-microgel interaction is to assume a potential of the form  $U(r) \sim r^{-n}$ . When the potential has this form, the dependence of  $G_p$  on  $\zeta$  is  $G_p \sim \zeta^{(1+n/3)}$ .

For the ULC microgels used here, a fit of the data in Fig. 2 leads us to estimate  $n_{ULC} = 7.7 \pm 0.2$ . Following the

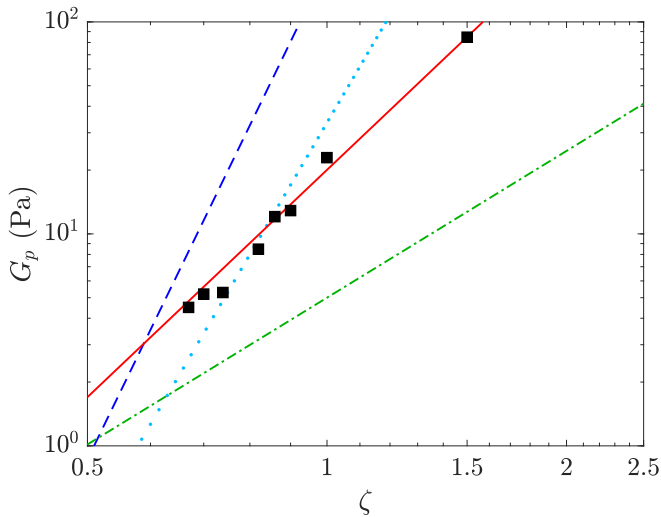


FIG. 2. Values of the plateau of the elastic modulus of solutions of ultralow cross-linked microgels,  $G_p$ , vs generalized volume fraction,  $\zeta$  (black squares). The red line represents the fit of the data using  $G_p \sim \zeta^{(1+n/3)}$ . The dashed, dotted, and dash-dotted lines represent the increase of  $G_p$  as a function of  $\zeta$  for 10 mol% and 1 mol% cross-linked microgels and linear polymer, respectively [27,30].

computer simulations in Refs. [1] and [20], the value of  $n_{\text{ULC}}$  leads to a prediction for the freezing point at 0.70 of the packing fraction, in excellent agreement with our system that has  $\zeta_f = 0.717 \pm 0.09$ .

$n_{\text{ULC}} = 7.7 \pm 0.2$  is comparable to the values obtained for other solutions of ULC microgels [27,30]. This value is significantly lower with respect to the exponent found for cross-linked microgels. As a comparison, the dashed and dotted lines represent the course of 10 and 1 mol% cross-linked microgels, respectively [27,30] that have  $n \approx 20$ . As a further comparison to the ULC microgels, the course for linear polymer is shown by the dash-dotted line,  $n_{\text{poly}} = 2.3$  [41]. Figure 2 highlights that the ULC microgels interact with a microgel-to-microgel potential softer than regular microgels but still harder than linear polymers.

## II. STRUCTURE FACTOR ANALYSIS: SMALL-ANGLE X-RAY SCATTERING

A more detailed characterization of the structures of the concentrated solutions, shown in Fig. 1(a), has been achieved using small-angle x-ray scattering. In these experiments, the scattered intensity,  $I(q)$ , is proportional to the product between the form factor,  $P(q)$ , and the structure factor,  $S(q)$ , which equals 1 in the limit of infinite dilution. The form factor contains all the information (size, polydispersity, shape, internal architecture) about the single scattering object. The structure factor depends on the particle-to-particle arrangement.

### A. Detector images

The images of the SAXS detector are shown in Fig. 3. The different panels correspond to the different generalized volume fractions of the solutions. The black circle in the

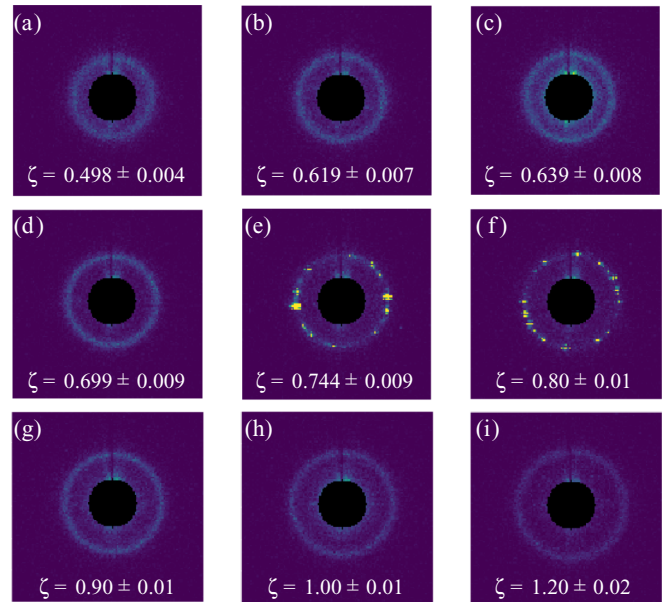


FIG. 3. Detector images acquired by SAXS measuring solutions of microgels with increasing generalized volume fraction ( $\zeta$ ) from panels (a) to (i). All samples have been measured at  $T = 20.0 \pm 0.1$  °C.

center of all the images is the mask used to cover the forward scattering of the direct beam in close proximity to the beam stop. In all the images, a light blue circle is visible. This corresponds to the values of the scattering vector,  $q$ , where it is most likely to find a microgel; in real space, this is the nearest neighbor distance,  $d_{nn}$ . With increasing concentration from  $0.498 \pm 0.004$ , Fig. 3(a), to  $1.20 \pm 0.02$ , Fig. 3(i), the radius of this circle increases. This corresponds to an increase of the scattering vector and, therefore, a decrease of  $d_{nn}$ .

Two examples of the scattering patterns of crystalline samples are shown in Figs. 3(e) and 3(f). Yellow spots, which correspond to higher intensity, are clearly visible over the underlying light blue circles. These dots are due to the scattering from the ordered lattices formed by the microgels. The presence of multiple dots relatively close to each other indicates that the samples present many polycrystalline domains with different orientations. Furthermore, the absence of a second ring of Bragg peaks indicates that these crystals are small and the order is limited to short length scales. Indeed, the absence of higher Bragg reflections has been reported in the literature for both microgels and hard sphere suspensions related to the presence of defects in the crystalline lattice mainly due to size mismatch between the particles forming the crystals [13,42].

### B. Intensities and structure factors

Figure 4 shows a series of  $I(q)$  for samples at different concentrations, from  $\zeta = 0.639 \pm 0.008$  (bottom) to  $\zeta = 1.20 \pm 0.02$  (top). Data are shifted in the y direction for clarity. These curves are obtained performing a two-dimensional (2D) integration of the images shown in Fig. 3 and have been background subtracted. The first observation is that in all the curves there is a clear peak corresponding to the light blue

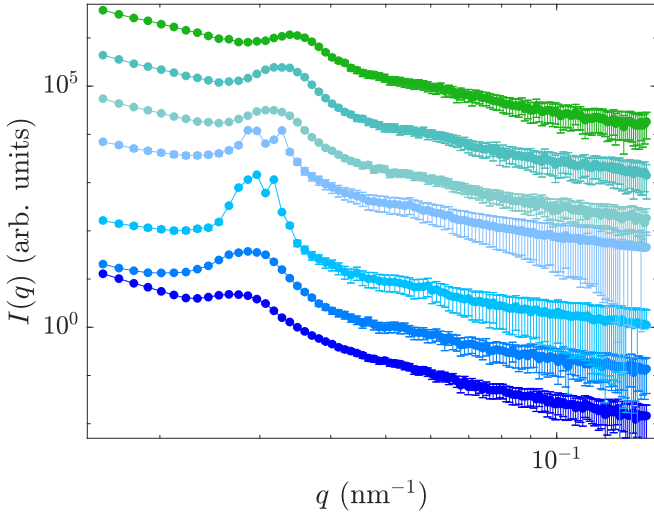


FIG. 4. SAXS intensities,  $I(q)$ , vs scattering vector,  $q$ , of solutions of microgels with increasing concentration from bottom to top:  $\zeta = 0.639 \pm 0.008$ ,  $\zeta = 0.699 \pm 0.009$ ,  $\zeta = 0.744 \pm 0.009$ ,  $\zeta = 0.80 \pm 0.01$ ,  $\zeta = 0.90 \pm 0.01$ ,  $\zeta = 1.00 \pm 0.01$ , and  $\zeta = 1.20 \pm 0.02$ . Data are shifted in the  $y$  direction for clarity.

circles observed in Fig. 3. These peaks shift to higher  $q$ , that is, smaller nearest-neighbor distance ( $d_{nn}$ ), with increasing the concentration of microgels in solution (from bottom to top). For liquid and glassy samples,  $d_{nn} \approx 2\pi/q_{\max}$ , with  $q_{\max}$  being the value of  $q$  corresponding to the maximum of the first peak [32,43]. For crystalline lattices,  $d_{nn}$  depends on the lattice constant, but this relation is different for different crys-

talline lattices. For instance, with  $a$  being the lattice constant,  $d_{nn} = a/\sqrt{2}$  for a face centered cubic (fcc) lattice, while for a body centered cubic crystal  $d_{nn} = a\sqrt{3}/2$ .

The peaks of the third and fourth  $I(q)$ s from the bottom corresponds to Figs. 3(e) and 3(f). The data clearly show Bragg peaks detected in the scattering experiment. As noted above, only first-order peaks are visible. This indicates that at short length scales the samples are strongly ordered and at larger length scales the order is lost: The crystals are relatively small and polycrystalline samples form with defects in the lattice [13,42].

Structure factors  $S(q)$  are obtained by dividing the measured intensities,  $I(q)$ , by the SAXS intensity of the ULC microgels measured in diluted solutions ( $\zeta < 0.05$ ) that is proportional to the form factor  $P(q)$  of the ultralow cross-linked microgels. This means that we are neglecting the possible deswelling and/or deformation of the microgels at high packing fractions. Nevertheless, it has been shown that this approach leads only to an error of  $\ll 5\%$  [13,18]. Since we are mainly interested in the features of the first peak, this procedure is therefore appropriate.

### C. Structure factor of disordered samples

Figure 5 shows the structure factors of the concentrated microgel solutions. We notice that, as expected, all the structure factors (blue squares) reach the plateau value of 1 (black horizontal lines) for high  $q$ .

The first two panels show the structure factors of liquid samples at packing fractions  $\zeta = 0.4980 \pm 0.004$  and  $\zeta = 0.619 \pm 0.007$ , Figs. 5(a) and 5(b), respectively. The red lines

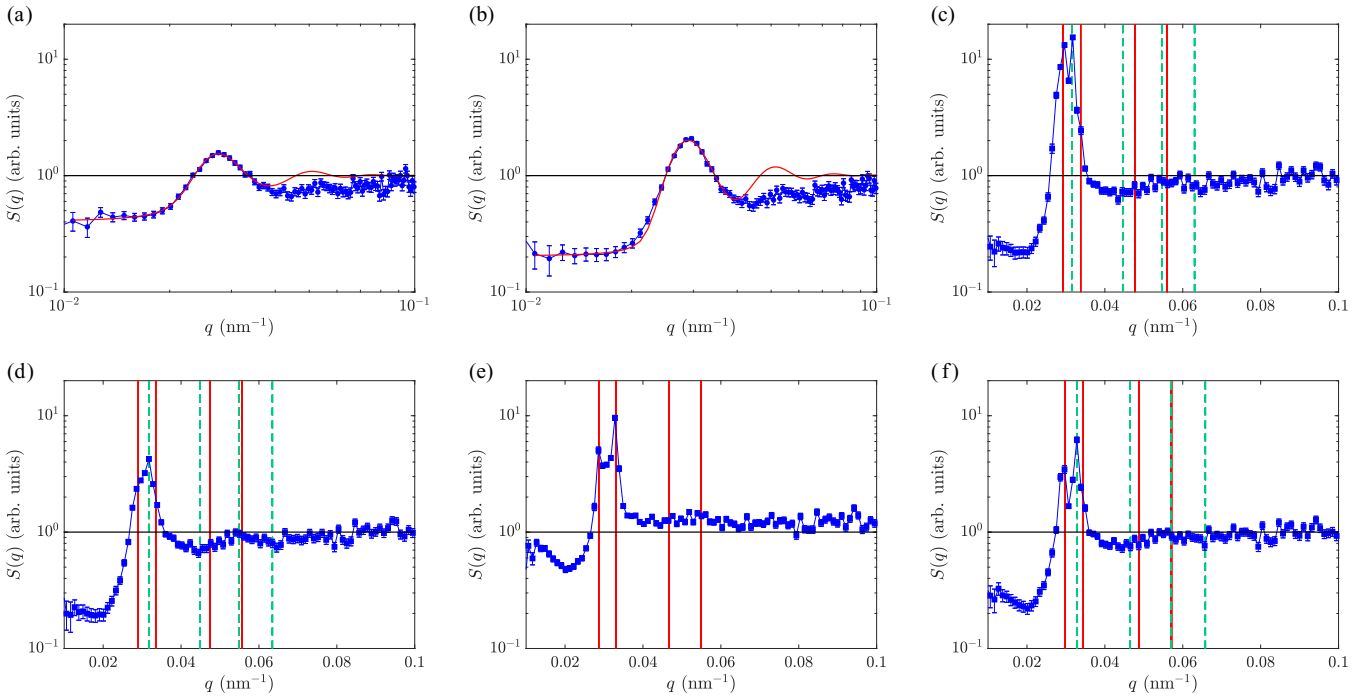


FIG. 5. Structure factor (blue squares) of solutions of ultralow cross-linked microgels at packing fractions equal to (a)  $\zeta = 0.4980 \pm 0.004$ , (b)  $\zeta = 0.619 \pm 0.007$ , (c)  $\zeta = 0.744 \pm 0.009$ , (d)  $\zeta = 0.758 \pm 0.009$ , (e)  $\zeta = 0.78 \pm 0.01$ , and (f)  $\zeta = 0.80 \pm 0.01$ . [(a), (b)] The red solid lines represent fits of the data with a Percus-Yevick structure factor [44]. [(c)–(f)] The vertical lines represent the expected positions of Bragg peaks for fcc (red) and bcc (dashed green) crystalline lattices. The horizontal black lines correspond to  $S(q) = 1$ .

represent fits of the data with the Percus-Yevick structure factor [44] where the microgel generalized packing fraction,  $\zeta_{PY}$ , and the radius of the microgels are fitting parameters. The fits have been performed using SASVIEW 4.2.2 software. This model has already been used to describe solutions of compressible microgels at low packing fraction [17,45,46]. It is clear that while the position and the intensity of the first peak of the structure factor is well reproduced by the model, the data are not reproduced for high  $q$ . This may be due to the rapid decrease of the order in the samples and to the fact that we are neglecting changes in the form factor depending on concentration. Other factors that can lead to this disagreement between the data and the model are the low contrast of the ULC microgels and the fact that the Percus-Yevick structure factor we are using is aimed for low concentrated solutions of hard spheres [47]. Nevertheless, the values obtained for the generalized volume fraction  $\zeta_{PY}$  are consistent with the value of  $\zeta$  obtained from viscosity measurements (Supplemental Material [29]). Furthermore, the nearest neighbor distance obtained from the fits are in good agreement with the  $d_{nm}$  obtained from  $q_{max}$ .

#### D. Structure factor of crystalline samples

Figures 5(c) to 5(f) correspond to the structure factors of the crystalline samples. As mentioned above, we notice that only the first Bragg peaks are visible, revealing the presence of small polycrystalline domains with different orientations within the samples and with a significant number of defects in the different lattices [13,42]. The vertical red lines represent the expected peak positions of microgels crystallizing in a fcc lattice. Except for the sample in Fig. 5(e), all the other structure factors contain additional peaks that cannot be related to an fcc lattice. The additional peaks can only be explained by the coexistence in the sample of crystals with a different lattice. While fcc is the equilibrium structure, microgel solutions can also crystallize in hexagonal or random hexagonal close-packed (hcp and rhcp, respectively) lattices since these structures are obtained by a different stacking of hexagonal planes [46] and are energetically very close to the fcc arrangement [48–50]. Therefore, we tried to reproduce the position of the additional peaks using either hcp or rhcp lattices. For both these crystalline structures, the lattice constants that reproduce the positions of the first peaks in Figs. 5(c), 5(d) and 5(f) lead to positions of second peaks which are not in agreement with the measured second peaks in the structure factors. This is due to the selection rules of the Bragg reflections for these lattices [51]. Therefore, hcp and rhcp lattices have been excluded.

Softness of the microgels can lead to the formation of crystals with unexpected lattices in comparison to hard spheres, e.g., metastable body centered cubic [46,52]. The first peak, marked by the first green dashed lines in Figs. 5(c), 5(d) and 5(f), is due to the reflection from the plane (1,1,0) in the conventional unit cell of bcc [51]. Despite the absence of higher order peaks, the presence of the bcc crystals is the most reasonable option since it leads to lattice constants comparable to the one of the fcc lattices and is in agreement with the SANS experiments presented later. Furthermore, the presence of a bcc lattice is supported by previous data in the literature related to solutions of soft microgels [46,52]. Nevertheless,

we highlight that while in Refs. [52] and [46] the bcc crystals were metastable, the extreme softness of the interaction potential between ULC microgels leads to the coexistence of two stable crystalline lattices, fcc and bcc, respectively.

### III. RESPONSE OF ULTRALOW CROSS-LINKED MICROGELS TO CROWDING: SMALL-ANGLE NEUTRON SCATTERING

To have further insight into the behavior of these ultrasoft microgels in solution, we now focus on the single microgel response to crowding. Recently, we have shown that the ultralow cross-linked microgels are significantly compressed once embedded in a matrix of regular microgels [28]. This study revealed that ULC microgels preferentially deswell, in contrast to microgels synthesized with the addition of a cross-linker agent that show a strong interpenetration of their neighbors [28]. The different response depends both on the difference in bulk moduli between the ultralow cross-linked and the regular microgels, but also on their different internal structures [27,28]. Here the response of ULC microgels embedded in a matrix of deuterated ( $[C_6D_3H_8NO]_n$ ), but otherwise identical, ULC microgels has been studied. The use of a matrix of deuterated microgels is essential to measure the single microgel signal, where  $I(q) \propto P(q)$ , in crowded environment by means of SANS with contrast variation. The measurements have been performed on the D11 instrument [53] at the Institut Laue-Langevin and on the KWS-1 [54] and KWS-2 [55] instruments operated by JCNS at the Heinz Maier-Leibnitz Zentrum (Supplemental Material [29]). In contrast to other studies [18,28,32,56,57], here it was necessary to use a deuterated monomer with only three atoms of deuterium and not seven. The reason for this is that in the D7-pNIPAM the isopropyl group of NIPAM is deuterated and consequently the cross linking is strongly restrained [26]. As a consequence, the formation of microgels using D7-pNIPAM is precluded.

#### A. Experimental determination of the match point

Since we used a different monomer ( $[C_6D_3H_8NO]_n$ ) with respect to the literature ( $[C_6D_7H_4NO]_n$ ) [18,28,32,56,57], the match point of the deuterated ULC microgels has been determined experimentally. Figure 6(a) shows the scattered intensities of highly diluted solutions of D3-ULC microgels as a function of the scattering vector,  $q$ , suspended in various  $D_2O/H_2O$  mixtures, namely 0, 20, 50, 60, 80, and 100 wt.%  $D_2O$ .

Clearly, with increasing the content of  $D_2O$  from 0 to 60 wt.%, the contrast get increasingly worse, as shown by Fig. 6(a). For the last two mixtures, 80 and 100 wt.%  $D_2O$ , the contrast is good again. Since all the solutions have the same concentration and contain the very same microgels, the only reason for the changes in the scattered intensities is due to variations of the scattering contrast between the deuterated microgels and the solvent,  $\Delta\rho$ . Therefore, to find  $\Delta\rho$ , different scattering vectors ( $q_1, q_2, \dots, q_5$ ) are selected [vertical lines in Fig. 6(a)] and the square root of the values of the corresponding  $I(q)$ s at different contrast are taken for each  $q_i$ , with  $i = 1 \dots 5$  [for diluted solutions  $I(q = q_i) \propto P(q =$

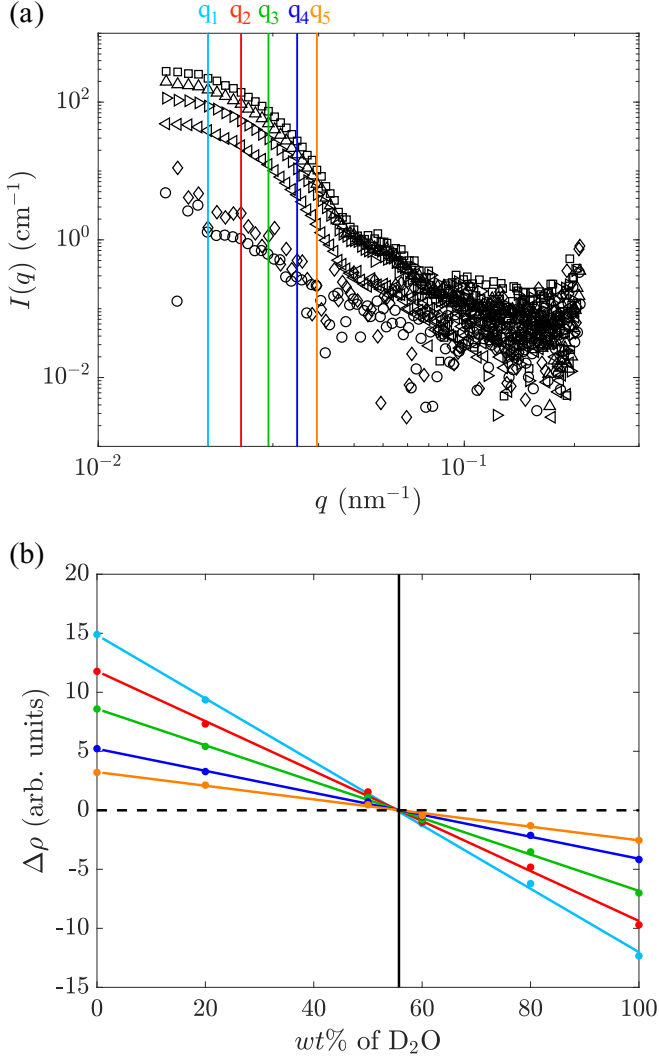


FIG. 6. (a) SANS intensity,  $I(q)$ , as a function of the scattering vector,  $q$ , of the deuterated-ULC microgels probed at  $20.0 \pm 0.1$  °C suspended in  $\text{D}_2\text{O}/\text{H}_2\text{O}$  mixtures with 100 wt.%  $\text{D}_2\text{O}$  (upward-pointing triangles), 80 wt.%  $\text{D}_2\text{O}$  (left-pointing triangles), 60 wt.%  $\text{D}_2\text{O}$  (circles), 50 wt.%  $\text{D}_2\text{O}$  (diamonds), 20 wt.%  $\text{D}_2\text{O}$  (right-pointing triangles), and 0 wt.%  $\text{D}_2\text{O}$  (squares). The colored vertical solid lines represent fixed  $q$  used to extract the contrast in panel (b). (b) Scattering length density contrast,  $\Delta\rho$ , as a function of the wt.% of  $\text{D}_2\text{O}$  in the solvent. The different colors corresponds to the different  $q$  chosen in panel (a) to extract the contrast. The solid lines represent linear fits of the data. The dashed black horizontal line shows the zero contrast line. The black solid vertical line represent the match point of the deuterated ULC microgels:  $55.7 \pm 0.3$  wt.%  $\text{D}_2\text{O}$ .

$q_i \simeq \Delta\rho^2$ ]. These values are plotted in Fig. 6(b). For the mixtures with 60, 80, and 100 wt.% of  $\text{D}_2\text{O}$ , the negative solutions for the contrast has been selected since the sign of  $\Delta\rho$  changes when the scattering length density of the solvent crosses the match point.

For every selected  $q$ , the variation of the values of  $I(q)$  depends on the variation of  $\Delta\rho$ . For all the chosen  $q$ , a linear fit is performed. All the fits cross the zero axes (dashed black line) in the very same point:  $55.7 \pm 0.3$  wt.%  $\text{D}_2\text{O}$ , that is,

TABLE I. Generalized volume fractions,  $\zeta$ , and fitting parameters as obtained from the fit of the SANS data. All the samples reported in the table have been measured at constant temperature ( $20.0 \pm 0.01$  °C). The corresponding fits and radial distributions are shown in Fig. 7 and the Supplemental Material [29].

$\zeta$	$R_{\text{SANS}}$ (nm)	$R_c$ (nm)	$2\sigma$ (nm)	$\xi$ (nm)	$\sigma_p$ (%)
$0.080 \pm 0.003$	$136 \pm 3$	$48 \pm 1$	$88 \pm 2$	$12 \pm 2$	$9.5 \pm 0.7$
$0.593 \pm 0.007$	$135 \pm 3$	$53 \pm 1$	$81 \pm 2$	$12 \pm 2$	$11 \pm 1$
$0.661 \pm 0.008$	$133 \pm 4$	$59 \pm 2$	$74 \pm 2$	$13 \pm 1$	$10.9 \pm 0.9$
$0.697 \pm 0.009$	$132 \pm 4$	$58 \pm 1$	$74 \pm 3$	$13 \pm 1$	$10.1 \pm 0.6$
$0.750 \pm 0.009$	$116 \pm 4$	$78 \pm 2$	$38 \pm 2$	$12 \pm 1$	$14.0 \pm 0.9$
$0.79 \pm 0.01$	$105 \pm 4$	$88 \pm 1$	$16 \pm 3$	$12 \pm 1$	$13.4 \pm 0.9$
$0.86 \pm 0.01$	$98 \pm 2$	$97 \pm 1$		$7 \pm 1$	$14 \pm 1$
$0.91 \pm 0.01$	$98 \pm 1$	$97 \pm 1$		$6 \pm 2$	$14 \pm 1$
$0.98 \pm 0.01$	$94 \pm 2$	$93 \pm 1$		$5 \pm 2$	$15 \pm 1$
$1.10 \pm 0.02$	$92 \pm 1$	$92 \pm 1$		$6 \pm 1$	$16 \pm 2$
$1.29 \pm 0.02$	$90 \pm 3$	$90 \pm 1$		$5 \pm 1$	$18 \pm 2$
$1.66 \pm 0.02$	$72 \pm 3$	$72 \pm 1$		$4 \pm 1$	$17 \pm 2$
$2.22 \pm 0.03$	$70 \pm 4$	$70 \pm 1$		$4 \pm 1$	$16 \pm 1$

the scattering length density of the deuterated ULC microgels. The samples for SANS with contrast variation have been prepared in this solvent. The scattering length density obtained experimentally is  $3.137 \times 10^{-6} \text{ \AA}^{-2}$ . The experimental value is very close to the theoretical value of  $2.949 \times 10^{-6} \text{ \AA}^{-2}$  calculated from the scattering lengths of the atoms composing the deuterated monomer [58]. The difference between the two values can be due to the incorporation of fragments of the initiators or to impurities in the deuterated monomer or solvent.

## B. Form factor analysis in crowded environments

The volume fraction of the hydrogenated ULC microgels,  $\zeta_H$ , is kept constant and equals  $0.080 \pm 0.003$  in all the samples measured with SANS with contrast variation. The generalized volume fraction of the deuterated microgels composing the matrix where the hydrogenated ULC microgels are embedded,  $\zeta_D$ , covers a range of concentrations between 0 and  $2.14 \pm 0.03$ . Consequently, the total generalized volume fraction,  $\zeta = \zeta_H + \zeta_D$ , covers a concentration range between 0.08 and  $2.22 \pm 0.03$ .

The data in Fig. 7(a) (and in the Supplemental Material [29]) are proportional to the form factors of the hydrogenated ULC microgels measured by SANS. The  $I(q)$ s in Fig. 7 are shifted in the  $y$  direction for clarity. The data are fitted using the model for a fuzzy sphere [59,60] (black solid lines), which has been shown to reproduce the form factors of ULC microgels [27,28]; therefore, this model has been chosen instead of newly developed routine for the data fitting [61,62]. The characteristic lengths of the microgels (total radius,  $R_{\text{SANS}}$ ; core radius,  $R_c$ ; and length of the fuzzy shell,  $2\sigma$ ) obtained from the fits of the data are used to plot the radial distribution of the relative polymer volume fraction within the microgel shown in Fig. 7(b) (and in the Supplemental Material [29]). The parameters obtained from the fits, together with the mesh size  $\xi$  and the size polydispersity  $\sigma_p$ , are shown in Table I.

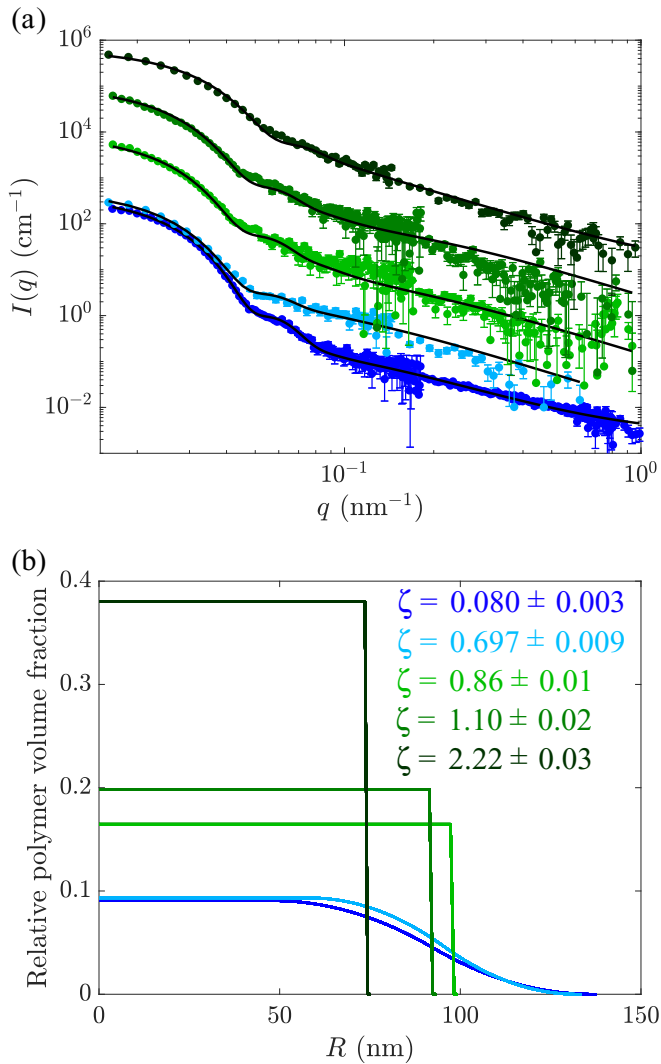


FIG. 7. (a) SANS intensity,  $I(q)$ , vs scattering vector,  $q$ , of the ultralow cross-linked hydrogenated microgels. Data are shifted in the y direction for clarity. (b) Radial distribution of the relative polymer volume fraction as obtained by fits of the curves in (a) using the model of Ref. [59]. In panel (a), the concentrations from bottom to top are  $\zeta = 0.080 \pm 0.003$ ,  $0.697 \pm 0.009$ ,  $0.86 \pm 0.01$ ,  $1.10 \pm 0.02$ , and  $2.22 \pm 0.03$ . All the measurements were performed at  $T = 20.0 \pm 0.01$  °C. The colors and concentrations in panel (b) correspond to those in panel (a).

The blue symbols in Fig. 7(a) represent the form factors of the hydrogenated ULC microgels in the dilute condition ( $\zeta \leq 0.080 \pm 0.003$ ), i.e., without the addition of deuterated ULC microgels. The total radius in the swollen state, at  $20.0 \pm 0.1$  °C, is  $136 \pm 3$  nm. This value is in agreement with the value of the hydrodynamic radius of the ULC microgels ( $R_h = 138.3 \pm 0.6$  nm) obtained from dynamic light scattering measurements of diluted solutions analyzed with second cumulant analysis [63,64]. The size polydispersity and the mesh size are  $\sigma_p = 9.5 \pm 0.7\%$  and  $\xi = 12 \pm 2$  nm.

When the concentration of the deuterated ULC microgels increases, a shift of the oscillation of the form factors can be observed in Fig. 7(a). The oscillation of the form factor of the hydrogenated microgels in the dilute condition is between

5 and  $8 \times 10^{-2}$   $\text{nm}^{-1}$ , blue symbols in the bottom curve. In contrast, the oscillation of the form factor for the sample at the highest concentration we measured,  $\zeta = 2.22 \pm 0.03$ , appears between 7 and  $9 \times 10^{-2}$   $\text{nm}^{-1}$ , dark green symbols in the top curve. Such a shift is compatible with a change in size and/or architecture of the microgels as a consequence of the increased concentration. The fits of the data for all the  $\zeta$  measured confirms this and the results are reported in Table I. The additional curves and fits are reported in the Supplemental Material [29].

The hydrogenated ULC microgels embedded in a matrix of deuterated, but otherwise identical, ULC microgels, maintain their size, almost unchanged up to a concentration of  $\zeta = 0.697 \pm 0.009$ . Not only the total size but also all the characterizing lengths of the microgel's internal structure ( $R_c$ ,  $2\sigma$ ,  $\xi$ ) are virtually the same, within the experimental errors. The radial profiles are shown in Fig. 7(b) according to the values reported in Table I. As can be seen, the radial profiles at concentrations  $\zeta \lesssim 0.7$  are all virtually the same (see Fig. 7(b) and the Supplemental Material [29]). This means that the ULC microgels are not compressed for moderate concentrations. This behavior is consistent with what is observed in the literature: microgels with comparable bulk moduli preferentially interpenetrate with their neighbors [28,32] or facets maintaining their volume constant [33,65] at moderate packing fractions.

When  $\zeta = 0.750 \pm 0.009$  the fit of the data shows that the ULC microgels are compressed and the radius is  $116 \pm 4$  nm (Table I). This compression is mainly due to the compression of the fuzzy external shell that decreases its length to  $38 \pm 2$  nm, almost half of the length with respect to the previous fits. A further increase in concentration leads to a more pronounced collapse of the ULC microgels and at  $\zeta = 0.86 \pm 0.01$ , the external fuzzy shell is completely collapsed, Fig. 7(b). For  $\zeta > 0.80$ , in Table I the length of the fuzzy shell is not indicated since the fits lead to values lower than 1 nm, which is below the SANS resolution.

With increasing  $\zeta$ , a constant decrease of the radius of the microgel is observed. This decrease holds until  $\zeta > 1.69$ . Above this value, the radii of the microgels seem to reach a constant value of  $\approx 70$  nm. This is shown in the curves corresponding to  $\zeta = 1.10 \pm 0.02$  and  $\zeta = 2.22 \pm 0.03$  in Fig. 7(b). The complete variation of the radial profiles for all the samples measured is shown in the Supplemental Material [29].

### C. Deformation and apparent polydispersity

An important point is that our model is assuming a spherical symmetry for the microgels. Nevertheless, super-resolved microscopy has shown that for other microgels, larger than those we are using in this study, faceting and deformations arise at high packing fraction [33,66]. As has been shown previously for nanoemulsion droplets, an increase of the fitting parameter related to the polydispersity is consistent with the deformation, and the consequent loss, of spherical symmetry [67]. Therefore, at high concentrations, this fitting parameter has to be interpreted as an apparent size polydispersity that accounts for the faceting of the scattering object.

Figure 8 shows the increase of the parameter  $\sigma_p$  as a function of  $\zeta$ . We think that the increase in the (apparent)

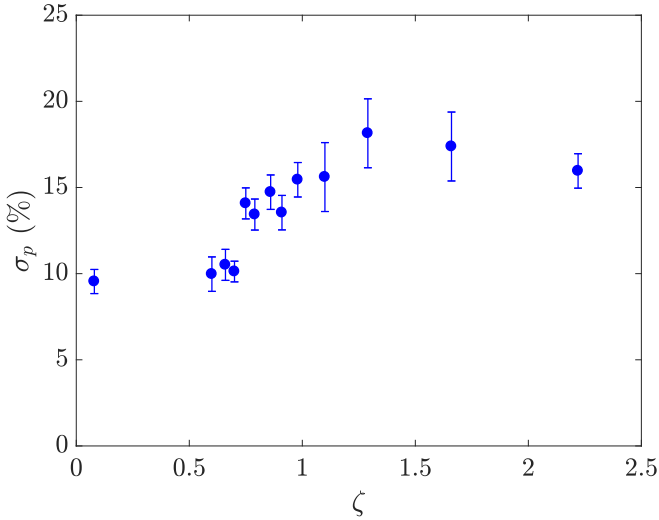


FIG. 8. Values of the fitting parameter  $\sigma_p$  as obtained from the fits in Fig. 7 and the Supplemental Material vs the generalized volume fraction.

polydispersity observed in our samples for  $\zeta > 0.74$  can be explained by the partial faceting of the ULC microgels. It should also be taken into account that the polymeric network of the ULC microgels does not possess a well-defined gradient of cross linker. This leads to a large variation in the bulk moduli between different ULC microgels, which in two dimensions has been shown to be responsible for the suppression of crystallization [27]. This fact, together with the observation that in bulk the softest microgels deswell at lower concentrations with respect to those with slightly larger bulk moduli [18,21,65], can also be the reason for the trend of the (apparent) polydispersity in Table I. Nevertheless, this increase in the (apparent) polydispersity is not suppressing the crystallization, as shown by the sample at  $\zeta = 0.750 \pm 0.009$  in Fig. 1(b).

#### D. Estimation of the volume fraction $\phi$

A general problem when dealing with soft deformable microgels is to access the real volume fraction,  $\phi$ , that is, the real volume occupied by the microgels in solution, and not the generalized volume fraction that does not account for osmotically induced size change. To address this problem, we can use the data on the size change of the microgels obtained with SANS with contrast variation. Nevertheless, as discussed in Sec. III C, the observed decrease in size for  $\zeta \gtrsim 0.74$  is accompanied by an increase in the parameter describing the polydispersity, indicating that the microgels are deviating from a spherical shape. This means that we cannot use the values of  $R_{\text{SANS}}$  to compute reliable values for  $\phi$  for  $\zeta \gtrsim 0.74$  since in this region deformation plays a role.

Nevertheless, we can compute the volume fraction for lower concentrations, in this case we have  $\phi = \zeta (R_{\text{SANS}}(\zeta)/R_{\text{SANS}}(\zeta = 0.080))^3$ . The values for  $\phi$  are reported in the Supplemental Material [29].

Figure 9 shows the course of the calculated  $\phi$  versus  $\zeta$  determined experimentally using the weight concentration of microgel in the solution and the conversion constant obtained from the viscosimetry measurements. As can be seen for low

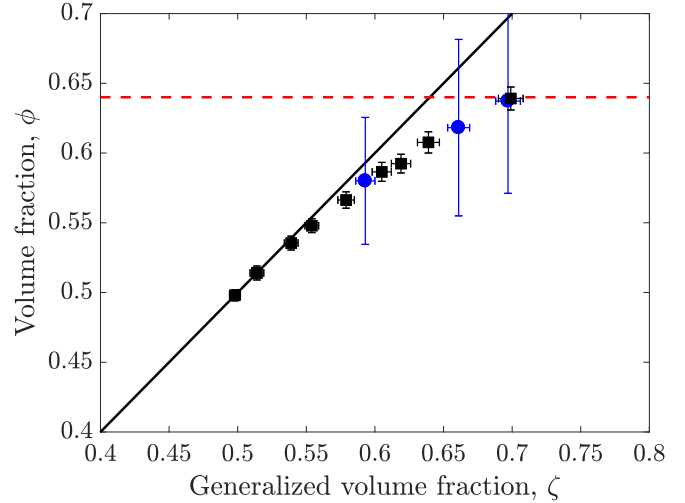


FIG. 9. Values of the volume fraction  $\phi$  computed using the sizes for the hydrogenated ultralow cross-linked microgels obtained by SANS vs the generalized volume fraction  $\zeta$ . Circles represent samples composed of a mixture of deuterated and hydrogenated microgels while the squares represent samples composed of hydrogenated microgels only. The solid black line corresponds to  $\phi = \zeta$  while the dashed red line represents the random close packing limit for hard spheres,  $\phi_{rcp} = 0.64$ .

concentrations,  $\zeta \lesssim 0.54$ , the data follow the line  $\phi = \zeta$ , solid black line. This means that the microgels do not change size, i.e., that the bulk modulus of the microgels in solution is larger than the solution osmotic pressure [18,25]. Then, at  $\zeta > 0.54$ , the data starts to deviate from this law indicating that osmotic-deswelling begins. It should be noted that the change in size happens well before the direct contact between the microgels ( $\phi_{rcp} = 0.64$ ), as already reported in the literature [18,21,25,67]. Finally, with increasing concentration the data seem to flatten at the value of the random close packing for hard spheres,  $\phi = 0.64$ ; see the dashed red line in Fig. 9. This is consistent with the fact that, once the concentration rises more, the microgels also have to change their shape to continue to fit in the available volume. The consequence of this is the increase of the parameter describing the polydispersity, as discussed in Sec. III C. Another point to notice is that crystals do not form for  $\phi < 0.64$ , this is in agreement with previous studies made on soft ionic microgels, where it was observed that softer microgels crystallize at higher packing fractions (not generalized), with respect to harder microgels and hard spheres [12].

#### IV. COMPARISON BETWEEN SMALL-ANGLE X-RAY AND NEUTRON SCATTERING

We notice that the crystals in the solution composed of a mixture of deuterated and hydrogenated ULC microgels appear at the same concentrations as the samples composed only by hydrogenated ULC microgels, i.e., the phase behavior of the different solutions is the same. This further confirms that the deuterated microgels are identical to the hydrogenated ULC microgels except for the presence of the three atoms of deuterium per NIPAM monomer. This allows us to directly compare the data we obtained from SAXS and from SANS.



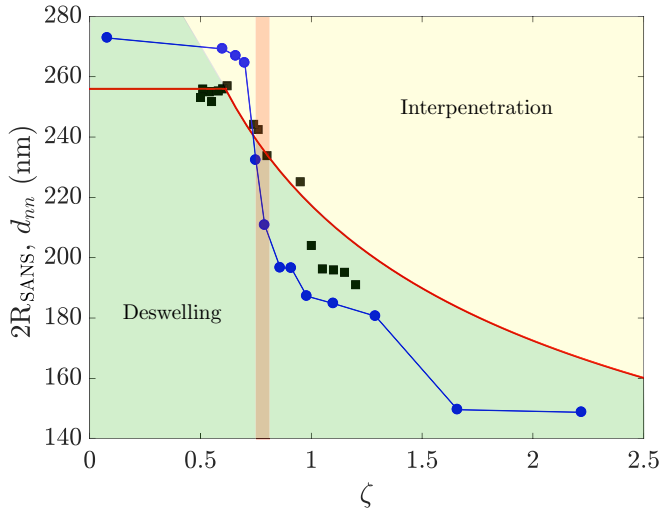


FIG. 10. Particle diameter  $2R_{\text{SANS}}$  (measured with SANS, blue circles) and nearest neighbor distance  $d_{mn}$  (measured with SAXS, black solid squares) vs generalized volume fraction  $\zeta$  for ultralow cross-linked microgel solutions. Red curve is a fit of the  $d_{mn}$  data for  $0.60 \gtrsim \zeta \gtrsim 1$  to the function  $c\zeta^{-1/3}$  with fit parameter  $c$ .

Figure 10 compares the nearest neighbors distance obtained from SAXS,  $d_{mn}$  (black squares), with the diameter of the hydrogenated ULC microgels embedded in the matrix of deuterated ultralow cross-linked microgels measured by SANS with contrast variation,  $2R_{\text{SANS}}$  (blue circles).

Let us consider first the behavior of  $d_{mn}$  as a function of the generalized volume fraction  $\zeta$ . For  $\zeta \lesssim 0.60$ , the nearest neighbor distance is constant: The red horizontal line is drawn at the average value  $\langle d_{mn} \rangle = 256$  nm. For  $0.60 \gtrsim \zeta \gtrsim 1$ , the data decrease as a function of  $\zeta^{-1/3}$ . This behavior is consistent with an isotropic deswelling of the particles as reported in the literature [13,18,32,57]. The red line in Fig. 10 is a fit of the data  $0.60 \gtrsim \zeta \gtrsim 1$ . For  $\zeta \gtrsim 1$ , the data show a compression that has a stronger dependence on  $\zeta$ . This can be explained by the deformation of the particles in response to the overcrowding.

Now let us focus on the values of the diameter of the ULC microgels. The blue circles that lie in the yellow area of Fig. 10 represent concentrations for which the ULC microgels have a diameter larger than the center-to-center distance between the microgels in the solution: At these concentrations, the microgels interpenetrate each other and maintain an external fuzziness (Fig. 7(b), Table I, and the Supplemental Material [29]).

In contrast, the blue circles in the green area of Fig. 10 represent solutions at  $\zeta$  where the diameter of the ultralow cross-linked microgels is smaller than the center-to-center distance between two neighbors; i.e., the microgels are deswollen and in contact with each other without (or with very limited) interpenetration and external fuzzy shell (Fig. 7(b), Table I, and the Supplemental Material).

As mentioned above, when microgels with different bulk moduli are mixed together the softest microgels deswell first with respect to microgels with slightly larger bulk moduli [18]. This mechanism allows for crystals to form at higher polydispersity with respect to hard spheres [13,21,65]. Ul-

tralow cross-linked microgels do not have a well-defined crosslink distribution, due to the absence of cross-linking agent during the synthesis. Consequences of this are the observed large differences in stretching of ULC microgels once adsorbed at the interfaces which reveal a significant variation of bulk moduli between different ULC microgels [24,25,27,68].

The red rectangular area in Fig. 10 represents the range of concentrations where the coexistence between stable bcc and fcc lattices has been observed. As can be seen in this region, we register the passage from interpenetration to deswelling. The two mechanisms are competing. In this region, ULC microgels with softer bulk moduli have a collapsed fuzzy shell while ULC microgels with a larger number of cross links or with a different topology of the network maintain a fuzzy periphery. This fact can be used to explain the variation of  $\sigma_p$  versus  $\zeta$  in Fig. 8 but also to understand the coexistence between bcc and fcc lattices.

Deswollen ULC microgels are similar to spheres without fuzziness. These systems obey the maximum packing fraction rule: To increase the configurational entropy of the system, they maximize the packing fraction due to pure excluded-volume interactions. For spheres in bulk, the maximum packing fraction is reached in a fcc lattice [48,69].

In contrast, particles with a less defined—fuzzy—periphery, such as the swollen ULC microgels, maximize their configurational entropy by increasing the contacts between neighbors [70]. This criterion has to be fulfilled since the particle-to-particle interaction for these systems scales with the contact area. In this scenario, the most efficient structure to maximize the contact area between neighbors is the bcc (or A15) lattice [70,71].

In the region of transition between fuzzy and collapsed ultralow cross-linked microgels, in the red area of Fig. 10, there are (deswollen) microgels which maximize their configurational entropy following the maximum packing fraction rule and other microgels (with external fuzziness) which maximize their configurational entropy, thus maximizing the contact area with their neighbors. The collapsed microgels form fcc crystals while the still fuzzy microgels form bcc crystals.

The coexistence in the solutions of microgels with slightly different sizes, due to the more or less pronounced collapse of their external fuzzy shell, is also consistent with the absence of higher Bragg reflections observed in the SAXS experiments. The crystals that these microgels form have different structures, fcc or bcc, but also incorporate a significant number of defects, due to the size mismatch. These defects have been recognized as the reason for the absence of a second ring of Bragg reflection [13,42].

## V. CONCLUSIONS

In this study, the phase behavior of supersoft spheres has been characterized. Our model system for supersoft spheres consists of solutions of ultralow cross-linked microgels. These microgels incorporate the lowest number of charges compared to microgels synthesized with the addition of cross-linker agents. Therefore, the effects of the counterions on the solution osmotic pressure [12,18,68] and, consequently, on the microgel phase behavior [13,24], are limited. This allows us

to study the phase behavior of soft spheres as a function of the packing fraction only.

The phase behavior presents the expected liquid-to-crystal transition and the formation of dense disordered states. The freezing and melting points are shifted to higher packing fractions,  $\zeta_f = 0.717 \pm 0.09$  and  $\zeta_m = 0.744 \pm 0.009$ , respectively. These values are significantly larger as compared to the typical values of  $\zeta_f = 0.56\text{--}0.58$  and  $\zeta_m = 0.61$  observed for other solutions of almost neutral microgels [13,19,35,37,38]. The shift of the boundaries of the liquid-to-crystal transition in our system is consistent with the prediction of computer simulation for particles interacting with very soft potentials [20].

The complex interplay between compression and interpenetration of the ultralow cross-linked microgels has been directly probed combining small-angle x-ray and neutron scattering with contrast variation to access both the particle-to-particle distance and the shape of the single microgels. These measurements reveal the coexistence between fcc and bcc stable lattices. The latter was observed as metastable lattice in solutions of stiffer microgels [46,52] or for nucleation of crystals of weakly charged colloids [72]. The stable bcc crystals are due to the fact that in the concentration range where crystals form, some of the ultralow cross-linked microgels maintain their fuzzy shell partially swollen. Therefore, because their interaction is dependent on the contact area with their neighbors, their configurational entropy is maximized by a bcc lattice [70].

Because of the easy synthetic protocol and the fine control over the size and size polydispersity, ultralow cross-linked microgels represent valid model systems for supersoft spheres

to investigate the role of softness on the crystallization process. They can be used in the future to investigate the prediction of the nucleation rate for soft spheres and compare it to the prediction for hard spheres [5,73]. Furthermore, ultralow cross-linked microgels can be used to investigate the glass and jammed states. We recently demonstrated that they can form both glass and jammed samples [30]. Even in this case, the advantage of using ULC microgels over other microgels is that the effects of charges and of osmotic deswelling are minimized.

All the data used for this paper are available, by request [74].

## ACKNOWLEDGMENTS

Authors are thankful to Dr. A. Menzel and to the EUSMI program for the help with the measurements performed on the cSAXS beamline of the Swiss Light Source, Paul Scherrer Institut. Financial support of the Deutsche Forschungsgemeinschaft (DFG) Project No. 191948804 within SFB 985 Functional Microgels and Microgel Systems, the International Helmholtz Research School of Biophysics and Soft Matter (IHRS BioSoft), is gratefully acknowledged. This work is based upon experiments performed at the D11 instrument at the Institut Laue-Langevin (ILL), Grenoble, France [75] and at the KWS-1 and KWS-2 instruments operated by JCNS at the Heinz Maier-Leibnitz Zentrum (MLZ), Garching, Germany. We also acknowledge the use of the free SASVIEW software for fitting the Perkus-Yevik model and the use of FITIT! for the fits of the form factors [76].

- 
- [1] W. Hoover and F. Ree, *J. Chem. Phys.* **49**, 3609 (1968).
  - [2] M. Baus, *J. Stat. Phys.* **48**, 1129 (1987).
  - [3] D. Frenkel, *J. Phys.: Condens. Matter* **6**, A71 (1994).
  - [4] P. N. Pusey and W. van Meegen, *Nature (London)* **320**, 340 (1986).
  - [5] U. Gasser, E. R. Weeks, A. Schofield, P. N. Pusey, and D. A. Weitz, *Science* **292**, 258 (2001).
  - [6] H. H. von Grünberg, P. Keim, K. Zahn, and G. Maret, *Phys. Rev. Lett.* **93**, 255703 (2004).
  - [7] U. Gasser, *J. Phys.: Condens. Matter* **21**, 203101 (2009).
  - [8] X. Ma, Z. S. Davidson, T. Still, R. J. S. Ivancic, S. S. Schoenholz, A. J. Liu, and A. G. Yodh, *Phys. Rev. Lett.* **122**, 028001 (2019).
  - [9] R. Pelton and P. Chibante, *Colloids Surf.* **20**, 247 (1986).
  - [10] M. Muluneh and D. A. Weitz, *Phys. Rev. E* **85**, 021405 (2012).
  - [11] D. Gottwald, C. N. Likos, G. Kahl, and H. Löwen, *Phys. Rev. Lett.* **92**, 068301 (2004).
  - [12] M. Pelaez-Fernandez, A. Souslov, L. A. Lyon, P. M. Goldbart, and A. Fernandez-Nieves, *Phys. Rev. Lett.* **114**, 098303 (2015).
  - [13] A. Scotti, U. Gasser, E. S. Herman, J. Han, A. Menzel, L. A. Lyon, and A. Fernandez-Nieves, *Phys. Rev. E* **96**, 032609 (2017).
  - [14] M. Cloitre, R. Borrega, and L. Leibler, *Phys. Rev. Lett.* **85**, 4819 (2000).
  - [15] M. Cloitre, R. Borrega, F. Monti, and L. Leibler, *Phys. Rev. Lett.* **90**, 068303 (2003).
  - [16] S. P. Meeker, R. T. Bonnecaze, and M. Cloitre, *Phys. Rev. Lett.* **92**, 198302 (2004).
  - [17] M. Stieger, J. S. Pedersen, P. Lindner, and W. Richtering, *Langmuir* **20**, 7283 (2004).
  - [18] A. Scotti, U. Gasser, E. S. Herman, M. Pelaez-Fernandez, L. A. Lyon, and A. Fernandez-Nieves, *Proc. Natl. Acad. Sci. U.S.A.* **113**, 5576 (2016).
  - [19] H. Senff and W. Richtering, *J. Chem. Phys.* **111**, 1705 (1999).
  - [20] R. Agrawal and D. A. Kofke, *J. Molecular Phys. B* **85**, 23 (1995).
  - [21] A. S. J. Iyer and L. A. Lyon, *Angew. Chem. Int. Ed.* **48**, 4562 (2009).
  - [22] D. Frenkel, *Nature (London)* **460**, 465 (2009).
  - [23] W. McPhee, K. C. Tam, and R. Pelton, *J. Colloid Interface Sci.* **156**, 24 (1993).
  - [24] M. Urich and A. R. Denton, *Soft Matter* **12**, 9086 (2016).
  - [25] U. Gasser, A. Scotti, and A. Fernandez-Nieves, *Phys. Rev. E* **99**, 042602 (2019).
  - [26] M. Brugnoli, A. C. Nickel, L. C. Kröger, A. Scotti, A. Pich, K. Leonhard, and W. Richtering, *Polym. Chem.* **10**, 2397 (2019).
  - [27] A. Scotti, S. Bochenek, M. Brugnoli, M. A. Fernandez-Rodriguez, M. F. Schulte, J. E. Houston, A. P. H. Gelissen, I. I. Potemkin, L. Isa, and W. Richtering, *Nat. Commun.* **10**, 1418 (2019).

- [28] A. Scotti, A. R. Denton, M. Brugnoli, J. E. Houston, R. Schweins, I. I. Potemkin, and W. Richtering, *Macromolecules* **52**, 3995 (2019).
- [29] See Supplemental Material at <http://link.aps.org/supplemental/10.1103/PhysRevE.102.052602> for more details about synthesis, microgel characterization, additional small-angle x-ray and neutron scattering data and analysis.
- [30] A. Scotti, M. Brugnoli, C. G. Lopez, S. Bochenek, J. J. Crassous, and W. Richtering, *Soft Matter* **16**, 668 (2020).
- [31] M. F. Schulte, A. Scotti, M. Brugnoli, S. Bochenek, A. Mourran, and W. Richtering, *Langmuir* **35**, 14769 (2019).
- [32] P. S. Mohanty, S. Nöjd, K. V. Gruijthuijsen, J. J. Crassous, M. Obiols-Rabasa, R. Schweins, A. Stradner, and P. Schurtenberger, *Sci. Rep.* **7**, 1487 (2017).
- [33] G. M. Conley, C. Zhang, P. Aebischer, J. L. Harden, and F. Scheffold, *Nat. Commun.* **10**, 2436 (2019).
- [34] J. Mattsson, H. M. Wyss, A. Fernandez-Nieves, K. Miyazaki, Z. Hu, D. R. Reichman, and D. A. Weitz, *Nature (London)* **462**, 83 (2009).
- [35] S. B. Debord and L. A. Lyon, *J. Phys. Chem. B* **107**, 2927 (2003).
- [36] G. K. Batchelor, *J. Fluid Mech.* **83**, 97 (1977).
- [37] S. Paulin, B. J. Ackerson, and M. Wolfe, *J. Colloid Interface Sci.* **178**, 251 (1996).
- [38] D. Paloli, P. S. Mohanty, J. J. Crassous, E. Zaccarelli, and P. Schurtenberger, *Soft Matter* **9**, 2927 (2013).
- [39] M. J. Bergman, N. Gnan, M. Obiols-Rabasa, J.-M. Meijer, L. Rovigatti, E. Zaccarelli, and P. Schurtenberger, *Nat. Commun.* **9**, 5039 (2018).
- [40] F. Scheffold, P. Díaz-Leyva, M. Reufer, N. Ben Braham, I. Lynch, and J. L. Harden, *Phys. Rev. Lett.* **104**, 128304 (2010).
- [41] M. Rubinstein and R. H. Colby, *Polymer Physics* (Oxford University Press, New York, 2003), Vol. 23.
- [42] S. Martin, G. Bryant, and W. van Meegen, *Phys. Rev. Lett.* **90**, 255702 (2003).
- [43] J. Liu, H.-J. Schöpe, and T. Palberg, *Part. Part. Syst. Charact.* **17**, 206 (2000).
- [44] J. K. Percus and G. J. Yevick, *Phys. Rev.* **110**, 1 (1958).
- [45] J. Wu, B. Zhou, and Z. Hu, *Phys. Rev. Lett.* **90**, 048304 (2003).
- [46] U. Gasser, J.-J. Lieter-Santos, A. Scotti, O. Bunk, A. Menzel, and A. Fernandez-Nieves, *Phys. Rev. E* **88**, 052308 (2013).
- [47] M. S. Wertheim, *Phys. Rev. Lett.* **10**, 321 (1963).
- [48] D. Frenkel and A. J. Ladd, *J. Chem. Phys.* **81**, 3188 (1984).
- [49] P. Bolhuis and D. Frenkel, *Phys. Rev. Lett.* **72**, 2211 (1994).
- [50] S. Pronk and D. Frenkel, *J. Chem. Phys.* **110**, 4589 (1999).
- [51] C. Kittel and P. McEuen, *Introduction to Solid State Physics*, 8th ed. (Wiley, New York, 1996).
- [52] P. Mohanty and W. Richtering, *J. Phys. Chem. B* **112**, 14692 (2008).
- [53] P. Lindner and R. Schweins, *Neutron News* **21**, 15 (2010).
- [54] A. V. Feoktystov, H. Frielinghaus, Z. Di, S. Jaksch, V. Pipich, M.-S. Appavou, E. Babcock, R. Hanslik, R. Engels, G. Kemmerling, *et al.*, *J. Appl. Crystallogr.* **48**, 61 (2015).
- [55] A. Radulescu, V. Pipich, H. Frielinghaus, and M.-S. Appavou, *J. Phys. Conf. Ser.* **351**, 012026 (2012).
- [56] U. Gasser, J. S. Hyatt, J.-J. Lieter-Santos, E. S. Herman, L. A. Lyon, and A. Fernandez-Nieves, *J. Chem. Phys.* **141**, 034901 (2014).
- [57] S. Nöjd, P. Holmqvist, N. Boon, M. Obiols-Rabasa, P. S. Mohanty, R. Schweins, and P. Schurtenberger, *Soft Matter* **14**, 4150 (2018).
- [58] F. S. Varley, *Neutron News* **3**, 29 (1992).
- [59] M. Stieger, W. Richtering, J. Pedersen, and P. Lindner, *J. Chem. Phys.* **120**, 6197 (2004).
- [60] I. Berndt, J. S. Pedersen, and W. Richtering, *J. Am. Chem. Soc.* **127**, 9372 (2005).
- [61] M. Cors, L. Wiehemeier, Y. Hertle, A. Feoktystov, F. Cousin, T. Hellweg, and J. Oberdisse, *Langmuir* **34**, 15403 (2018).
- [62] M. Cors, L. Wiehemeier, O. Wrede, A. Feoktystov, F. Cousin, T. Hellweg, and J. Oberdisse, *Soft Matter* **16**, 1922 (2020).
- [63] D. E. Koppel, *J. Chem. Phys.* **57**, 4814 (1972).
- [64] W. Burchard and W. Richtering, in *Relaxation in Polymers*, edited by M. Pietralla and W. Pechhold, Progress in Colloid and Polymer Science Vol 80 (Steinkopff, 1989).
- [65] I. Bouhid de Aguiar, T. van de Laar, M. Meireles, A. Bouchoux, J. Sprakel, and K. Schroën, *Sci. Rep.* **7**, 10223 (2017).
- [66] G. M. Conley, P. Aebischer, S. Nöjd, P. Schurtenberger, and F. Scheffold, *Sci. Adv.* **3**, e1700969 (2017).
- [67] F. Scheffold and T. Mason, *J. Phys.: Condens. Matter* **21**, 332102 (2009).
- [68] A. R. Denton and Q. Tang, *J. Chem. Phys.* **145**, 164901 (2016).
- [69] R. Higler, J. Appel, and J. Sprakel, *Soft Matter* **9**, 5372 (2013).
- [70] P. Zihlerl and R. D. Kamien, *Phys. Rev. Lett.* **85**, 3528 (2000).
- [71] P. Zihlerl and R. D. Kamien, *J. Phys. Chem. B* **105**, 10147 (2001).
- [72] S. Auer and D. Frenkel, *J. Phys.: Condens. Matter* **14**, 7667 (2002).
- [73] S. Auer and D. Frenkel, *Nature (London)* **409**, 1020 (2001).
- [74] A. Scotti *et al.*, Dataset for “Phase behavior of ultrasoft spheres show stable bcc lattices”, <https://moped.ecampus.rwth-aachen.de/proxy/apps/resolvehandle?pid=21.11102/c56fba01-afda-11ea-afb2-e41f1366df48> (2020).
- [75] A. Scotti, B. Monia, R. Walter, M. Friederike Schulte, and S. Ralf, Form factor of ultra-low crosslinked microgels in over-crowded environments, doi: 10.5291/ILL-DATA.9-10-1580, Institut Laue-Langevin (ILL), 2020.
- [76] <http://www.sasview.org/>; [www.github.com/ovirtanen/fitit](http://www.github.com/ovirtanen/fitit).